Comparison of Surface Permanent Magnet Axial and Radial Flux Coaxial Magnetic Gears

Matthew C. Gardner, *Student Member, IEEE*, Matthew Johnson, *Member, IEEE*, and Hamid A. Toliyat, *Fellow, IEEE*

***Abstract*—This paper provides a thorough, parametric comparison of axial and radial flux coaxial magnetic gears with surface-mounted permanent magnets (PMs). While both topologies share similar operating principles and can achieve comparable shear stresses, they exhibit different scaling trends with respect to key design parameters. Both topologies' volumetric torque densities (VTDs) increase with the outer radius, but the axial flux topology's VTD increases with the radius at a much faster rate than the radial flux topology's VTD. Another difference between the topologies involves their cross-sectional scaling parameters. The stack length axially scales radial flux gear cross-sections, and, as it increases, the impact of end-effects decreases, which improves the performance. For axial flux gears, the radii ratio scales the cross-section's radial width between different radii. This fundamentally changes optimal parameter values and design performance tradeoffs. Finally, axial flux rotors experience significant axial forces, but the radial forces on radial flux rotors can be balanced out. Based on these trends, radial flux gears are superior to axial flux gears for most applications; however, axial flux gears have a significant advantage when a large radius and a small axial length are permissible or when mechanical power needs to be transmitted across a flat barrier.**

***Index Terms*—Axial flux, end-effects, finite element analysis, gear ratio, magnetic gear, permanent magnet, radial flux, scaling, shear stress, torque density.**

I. Introduction

MAGNETIC gears convert energy between low-speed, high-torque rotation and high-speed, low-torque rotation. Thus, like mechanical gears, magnetic gears allow a relatively small, high-speed electric machine to connect to a low-speed system. However, unlike mechanical gears, magnetic gears transfer power using modulated magnetic fields instead of direct contact between mechanical teeth. This contactless operation provides numerous potential benefits, such as improved reliability, reduced maintenance, reduced acoustic noise, and physical isolation between shafts. Thus, magnetic gears have generated significant interest over the past two decades [1]-[3] and have been proposed for numerous applications, including wind [4] and wave [5], [6] energy harvesting, traction [7], and ship propulsion [8].

Most of the existing magnetic gear literature focuses on the radial flux coaxial magnetic gear [1]-[8], which is shown with surface-mounted permanent magnets (PMs) in Fig. 1(a). However, the axial dual of this topology, which is shown in Fig. 1(b) has also received some attention [9]-[13]. Although magnetic gears of either topology can be used as standalone gears, several magnetically geared machine (MGM) topologies integrate a radial or axial flux coaxial magnetic gear with an electric machine to form a single compact device [14]-[17]. Information about prototype designs and experimental results can be found in [2], [5], [7], [15], [18]-[20] for radial flux magnetic gears and MGMs and in [13], [16], [17] for axial flux magnetic gears and MGMs. Coaxial magnetic gears consist of two rotors with PMs (Rotors 1 and 3) and another rotor with magnetically soft poles called modulators (Rotor 2). For both topologies, the number of

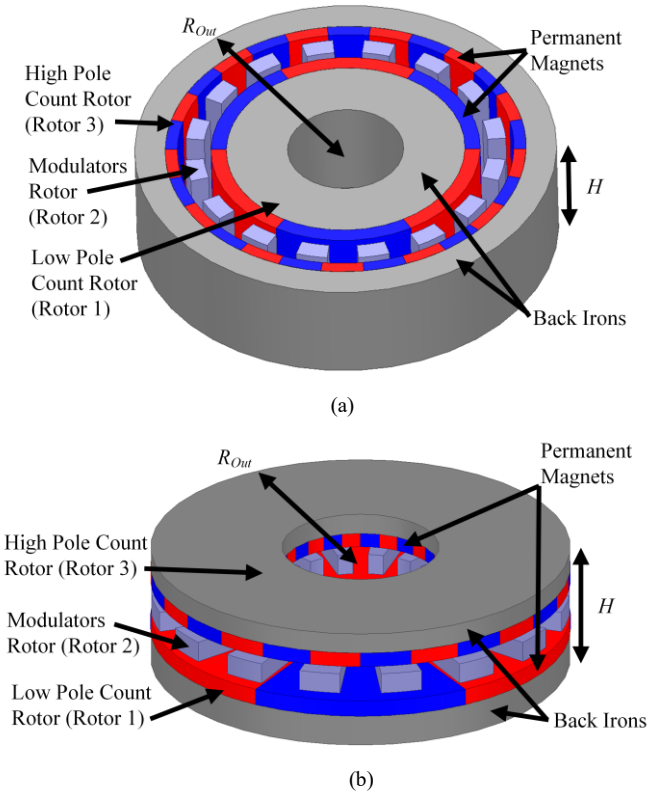

Fig. 1. (a) Radial flux and (b) axial flux coaxial magnetic gears with surface-mounted permanent magnets.

This work was supported in part by a Texas A&M Energy Institute Fellowship.

M. C. Gardner is with the Department of Electrical and Computer Engineering, Texas A&M University, College Station, TX 77843 USA (e-mail: gardner1100@tamu.edu).

M. Johnson was with the Department of Electrical and Computer Engineering, Texas A&M University, College Station, TX 77843 USA (e-mail: mjohnson11@tamu.edu).

H. A. Toliyat is with the Department of Electrical and Computer Engineering, Texas A&M University, College Station, TX 77843 USA (e-mail: toliyat@tamu.edu).

modulators (Q_2) should be the sum of the number of pole pairs on Rotor 1 (P_1) and Rotor 3 (P_3) [1]-[6], [18], as shown in

$$Q_2 = P_1 + P_3. \quad (1)$$

While multiple operating modes are possible, the highest gear ratio is achieved if the high pole count PM rotor (Rotor 3) is held stationary. In this case, the gear ratio (G) is given by

$$G = \frac{\omega_1}{\omega_2} = \frac{Q_2}{P_1}, \quad (2)$$

which relates the steady state speeds of Rotor 1 (ω_1) and Rotor 2 (ω_2) [3], [4], [6], [18]. Throughout this study, Rotor 3 is held stationary and Rotor 2 is used as the low speed rotor.

Although the fundamental operating principles of both topologies are similar, there are some important design, performance, and scaling differences. First, for radial flux gears, the radial magnetic forces on each rotor can be canceled out with symmetry [5], [21], [22]. Alternatively, in axial flux gears, symmetry cancels out the off-axis torques, but there are still unbalanced net axial magnetic forces on the rotors [17]. Second, the two topologies' performances scale differently, as summarized by [17] and in Table I (which is a simplistic but useful idealistic analysis based on the assumption of a fixed air gap shear stress, σ). Whereas the lever arm (the perpendicular distance between the axis of rotation and the location where the force is produced) is proportional to the radius for both topologies, the air gap area of the radial flux gear is approximately proportional to the product of its outer radius (R_{Out}) and axial height (H), but the air gap area of the axial flux gear is proportional to the outer radius squared. Thus, the volumetric torque density (VTD), which is the Rotor 2 stall torque (τ_2) divided by the active volume, as given by

$$VTD = \frac{\tau_2}{\pi \cdot R_{Out}^2 \cdot H}, \quad (3)$$

scales differently for the two topologies. The axial flux gear's VTD ideally grows linearly with the outer radius, but the radial flux gear's VTD is ideally invariant with outer radius. Therefore, the axial flux gear favors a form factor with a large outer radius and short axial height, but the radial flux gear's VTD is ideally much less dependent on form factor.

Although this qualitative finding is unsurprising given that it is a generally accepted fact for other more conventional axial and radial flux electric machines, it is also of limited value without a more detailed numeric characterization of these trends. However, to this point, only a single limited direct comparison has been made between axial flux and radial flux magnetic gears. Furthermore, because that study only compares designs at a single outer radius and axial length, it draws conclusions that contradict the aforementioned theoretically predicted and conventionally accepted form factor trends [23]. This study provides a thorough quantitative comparison of radial flux and axial flux coaxial magnetic gears with surface PMs by comparing optimal designs for different operating points and performance metrics. Additionally, this study evaluates and characterizes the scaling behaviors of both radial flux and axial flux coaxial magnetic gears. As with any design study, the exact numerical results presented in this paper depend on its assumptions, such as the use of a fixed air gap regardless of the design's radius or topology, but, due to the breadth of the parametric designs considered, the results still provide useful general indications of the two topologies' relative merits and design trend differences, which can be used to draw general conclusions and provide guidance at the outset of design specific studies.

TABLE I
Comparison of Ideal Geometrical Scaling Trends for Radial Flux and Axial Flux Magnetic Gears

Parameter	Radial Flux Gear	Axial Flux Gear
Air Gap Area	$\propto R_{Out} \cdot H$	$\propto R_{Out}^2$
Lever Arm	$\propto R_{Out}$	$\propto R_{Out}$
Torque	$\propto \sigma \cdot R_{Out}^2 \cdot H$	$\propto \sigma \cdot R_{Out}^3$
Volume	$\propto R_{Out}^2 \cdot H$	$\propto R_{Out}^2 \cdot H$
VTD	$\propto \sigma$	$\propto \sigma \cdot R_{Out}/H$

II. Design Study Methodology

To compare the two topologies, a broad parametric simulation sweep was performed for both topologies using nonlinear finite element analysis (FEA). Tables II-IV specify the parametric design combinations considered in this study, which were selected based on the results of past studies [17], [24], [25] in order to include a reasonable range and resolution of values for the most significant and interesting parameters. Table II provides the common ranges of values considered for each parameter used in both gear topologies, while Table III provides the ranges considered for each parameter unique to either of the two topologies. As in [17], [24], [25], a few derived parameters were used to facilitate the parametric sweep. First, G_{Int} represents the integer part of the gear ratio and determines the Rotor 3 pole pair count, P_3, in terms of the Rotor 1 pole pair count, P_1, according to

$$P_3 = \begin{cases} (G_{Int} - 1) \cdot P_1 + 1 & \text{for } G_{Int} \cdot P_1 \text{ odd} \\ (G_{Int} - 1) \cdot P_1 + 2 & \text{for } G_{Int} \cdot P_1 \text{ even} \end{cases}. \quad (4)$$

This formula allows the gear ratio to be maintained near a desired integer value as P_1 is varied, while simultaneously achieving two objectives. First, (4) results in a relatively high least common multiple between $2 \cdot P_1$ and Q_2, which keeps the cogging torque relatively low. Second, (4) ensures that Q_2 is even, which results in symmetry. For radial flux gears, this symmetry ideally cancels out the net radial forces on each rotor (assuming zero tolerances and no eccentricity). For axial flux gears, the symmetry ideally cancels out the off-axis torques on each rotor.

The second derived parameter, k_{PM}, which is the magnet thickness ratio, relates the thicknesses of the magnets on Rotor 1 (T_{PM1}) and Rotor 3 (T_{PM3}) according to

$$T_{PM3} = k_{PM} \cdot T_{PM1}. \quad (5)$$

Because Rotor 3 has more poles than Rotor 1, Rotor 3 experiences more flux leakage between adjacent poles, so it is generally optimal for the Rotor 1 magnets to be thicker than

the Rotor 3 magnets [25]. However, if the Rotor 1 magnets are too much thicker, they may demagnetize the Rotor 3 magnets. Thus, k_{PM} is varied between 0.5 and 0.75.

The third derived parameter, k_R, determines the radii ratio of the axial flux gears according to

$$R_{In} = k_R \cdot R_{Out}, \tag{6}$$

where R_{In} is the inner radius and R_{Out} is the outer radius. As indicated in Table III, this relationship is only used for the axial flux gears because the radii ratio for each radial flux gear is determined by R_{Out} and the radial thicknesses of the radial layers. Similarly, the axial height of each axial flux gear is determined by the various axial layer axial thicknesses, instead of an additional stack length parameter.

In addition to the parameters shown in Tables II and III, Table IV summarizes the various P_1 values evaluated for each G_{Int}, R_{Out}, and topology combination to ensure that the optimal P_1 value for each performance metric is within the range considered for each scenario, without including unnecessary sub-optimal cases. As G_{Int} is increased, the ratio of P_3 to P_1 increases according to (4). Thus, for higher values of G_{Int}, the optimal P_1 values are lower to prevent excessively short Rotor 3 pole arcs, which result in high leakage flux between adjacent poles. Similarly, larger R_{Out} values increase the pole arcs for a given pole count and lead to higher optimal P_1 values. Even values of P_1 were excluded to reduce the case count.

Magnetic performance is generally optimized by simply minimizing the air gap, so only a single air gap value was used in this study. In practice, the minimum viable air gap (from a mechanical design and manufacturing cost standpoint) should generally be used; however, this value may change depending on the outer radius and topology. Similarly, the results of past studies [25], [26] consistently indicate that the magnetically optimal modulator thicknesses tend to be smaller than the minimum mechanically practical thicknesses, so only a single modulator thickness was considered in this study. In practice, the minimum mechanically acceptable modulator thickness should generally be used in most designs. Furthermore, as shown in Fig. 1, all PM tangential fill factors were set to 1, and the modulator tangential fill factors were set to 0.5. More information about the generally less complex effects of these parameters can be found in [25]. Finally, some parameter value combinations from Table II would result in radial flux gears with negative inner radii, so these combinations were discarded from the radial flux gear design set.

Each design case was simulated using nonlinear FEA. For both the radial flux and axial flux designs, the PMs are made of NdFeB N42 with a remanent flux density of 1.3 T, the back irons are made of isotropic M47 magnetic steel, and the modulators are made of a soft magnetic composite, Somaloy 700 3P. All 5928 of the radial flux designs were simulated using 2D FEA, then 2481 of the best designs were simulated at each of the 11 different stack lengths specified in Table III using 3D FEA. All of the radial flux gear results presented in the following sections are based on 3D FEA unless specifically indicated otherwise. All 34,560 of the axial flux designs were simulated using 3D FEA exclusively.

TABLE II
Common Cross-Sectional Parameter Sweep Ranges

Parameter	Values	Units
Integer part of gear ratio (G_{Int})	4, 9, 16	
Outer radius (R_{Out})	50, 75, 100, 150, 200	mm
Rotor 1 back iron thickness (T_{BI1})	5, 10, 20	mm
Rotor 3 back iron thickness (T_{BI3})		
For T_{BI1} = 5 mm	5	mm
For T_{BI1} = 10 mm	5, 10	mm
For T_{BI1} = 20 mm	5, 10, 20	mm
Rotor 1 PM thickness (T_{PM1})	3, 6, 9, 12, 15	mm
PM thickness ratio (k_{PM})	0.5, 0.625, 0.75	
Air gap thicknesses (T_{AG})	1	mm
Modulator thickness (T_{Mods})	10	mm

TABLE III
Topology Specific Parameter Sweep Ranges

Parameter	Radial Flux Gear	Axial Flux Gear	Units
Radii ratio (k_R)	N/A	0.25, 0.375, …, 0.875	
Stack length (H)	5, 10, 15, 20, 25, 30, 40, 50, 60, 80, 100	N/A	mm

TABLE IV
Rotor 1 Pole Pair Count (P_1) Sweep Ranges

R_{Out} (mm)	G_{Int} = 4 (Radial)	G_{Int} = 4 (Axial)	G_{Int} = 9 (Radial)	G_{Int} = 9 (Axial)	G_{Int} = 16 (Radial)	G_{Int} = 16 (Axial)
50	3, 5, 7	3, 5, 7	3, 5, 7	3, 5, 7	3, 5	3, 5
75	3, 5, 7, 9	3, 5, 7, 9	3, 5, 7, 9	3, 5, 7	3, 5	3, 5
100	3, 5,… 11	3, 5,… 11	3, 5,… 11	3, 5, 7, 9	3, 5	3, 5
150	3, 5,… 19	3, 5,… 17	3, 5,… 13	3, 5,… 11	3, 5, 7	3, 5, 7
200	3, 5,… 23	3, 5,… 21	3, 5,… 15	3, 5,… 13	3, 5, 7, 9	3, 5, 7, 9

The designs are evaluated primarily based on three metrics: volumetric torque density (VTD), PM gravimetric torque density (PM GTD), and average air gap shear stress in the low speed air gap between Rotor 2 and Rotor 3 (σ_{LSAG}). VTD normalizes the torque of the magnetic gear based on its size as shown in (3). PM GTD is the Rotor 2 stall torque divided by the total mass of the PMs in the gear, as given by

$$PM\ GTD = \frac{\tau_2}{m_{PM}}, \tag{7}$$

where m_{PM} is the total mass of the PMs in the gear. PM GTD provides a normalized measure of how effectively each design uses the magnet material, which is the dominant source of active material cost in gears using NdFeB magnets [24]. Shear stress is a useful, but slightly more abstract, metric that characterizes the average tangential (torque producing) force per unit of air gap area yielded by a given design, without considering the lever arm (radius) at which that force is generated [27], [28]. This is useful for comparing the effects of design parameters besides outer radius on the performances of designs at different outer radius values. For radial flux designs, $\sigma_{LSAG,Rad}$ is given by

$$\sigma_{LSAG,Rad} = \frac{\tau_3}{2\pi \cdot R_{LSAG}^2 \cdot H}, \tag{8}$$

where R_{LSAG} is the radius of the low speed air gap and τ_3 is the

Rotor 3 stall torque. Similarly, for axial flux designs, $\sigma_{LSAG,Ax}$ is given by

$$\sigma_{LSAG,Ax} = \frac{\tau_3}{\frac{2\pi}{3}\cdot\left(R_{Out}^3 - R_{In}^3\right)}. \quad (9)$$

III. Results

A. 2-D Cross-Sectional Design Parameters

Figs. 2 – 15 illustrate several important design trends based on the parametric FEA simulation study results. In particular, Figs. 3, 4, and 6 depict the variation of the maximum VTD and PM GTD with some of the more impactful 2-D cross-sectional design parameters, T_{PM1}, P_1, and G_{Int}, for the various R_{Out} value and topology combinations denoted in the legend in Fig. 2. Fig. 3 shows the effects of varying the Rotor 1 permanent magnet (axial or radial) thickness on the maximum achievable VTD and PM GTD. The results in Fig. 3(a) demonstrate that, for most radial flux gears, the VTD is maximized by simply using the thickest magnets considered in the study, which is consistent with findings from previous studies [24], [25]. The lone exception to this trend in Fig. 3(a) is the 50 mm outer radius design set, where the decreased radial space limits the amount of magnet material that can be used effectively. If even thicker magnets were considered in this study, the finite radial space would eventually limit the optimal magnet thicknesses for radial flux gears with larger outer radii. When the available radial space is not an issue, this trend occurs because increasing the radial thickness of the

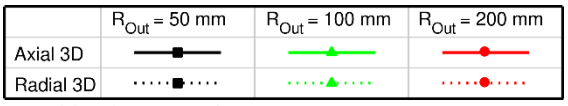

Fig. 2. Legend for Figs. 3, 4, and 6.

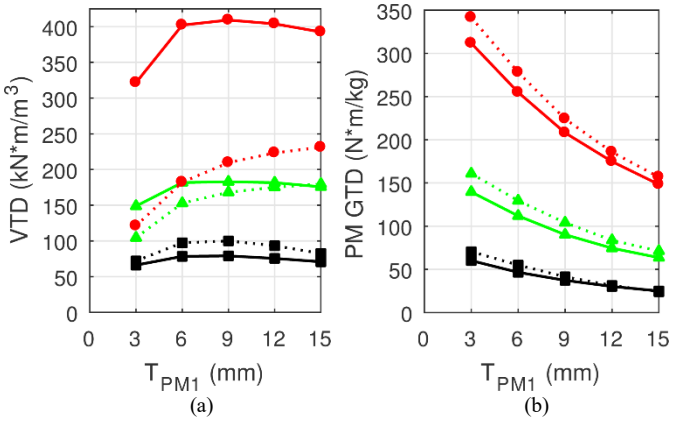

Fig. 3. Variation of maximum (a) VTD and (b) PM GTD with the Rotor 1 PM thickness for both axial flux gears and 50 mm stack length radial flux gears at different outer radius values (both with $G_{Int} = 4$).

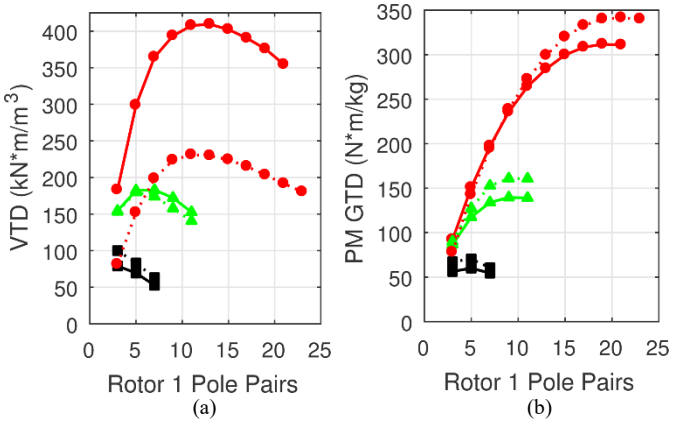

Fig. 4. Variation of maximum (a) VTD and (b) PM GTD with the Rotor 1 pole pair count for both axial flux gears and 50 mm stack length radial flux gears at different outer radius values (both with $G_{Int} = 4$).

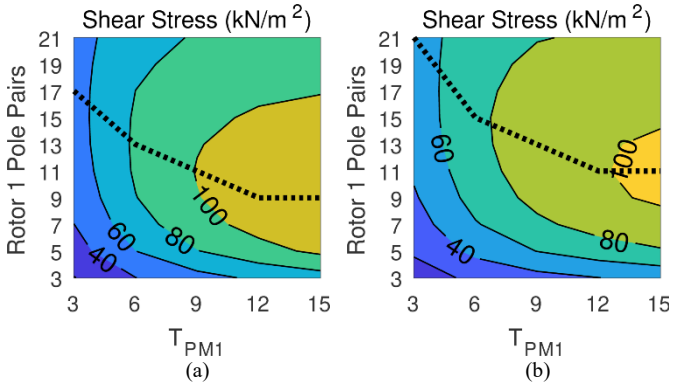

Fig. 5. Variation of maximum average low speed air gap shear stress with Rotor 1 PM thickness and pole pair count for (a) axial flux gears and (b) 50 mm stack length radial flux gears (both with a 200 mm outer radius and $G_{Int} = 4$). The dashed line indicates the optimal Rotor 1 pole pair count for each Rotor 1 PM thickness.

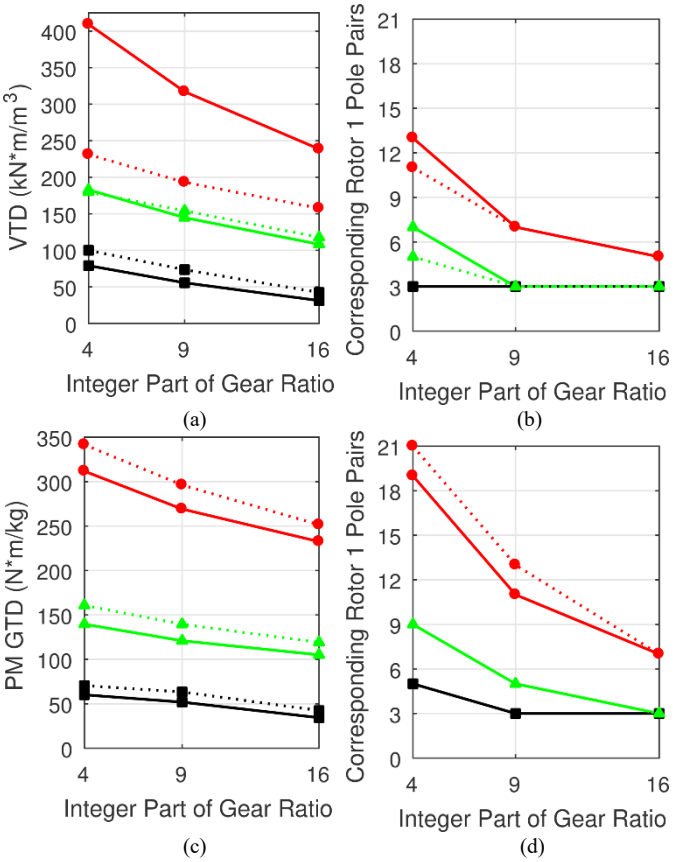

Fig. 6. Variation of (a) maximum VTD, (b) the corresponding optimum Rotor 1 pole pair count for maximizing VTD, (c) maximum PM GTD, and (d) the corresponding optimum Rotor 1 pole pair count for maximizing PM GTD with G_{Int} at different outer radius values for both axial flux gears and 50 mm stack length radial flux gears.

magnets does not increase the volume of the radial flux gears (for a fixed outer radius). However, because increasing the magnet thickness increases the effective air gap, the torque density returns diminish as magnet thickness continues to increase. As a result, the axial flux gear's behavior is more complicated. Increasing the axial thickness of the magnets in an axial flux gear is not a very effective means of increasing a design's torque rating, because it also increases the effective air gap. Furthermore, increasing the axial thickness of the magnets in the axial flux gear also increases the gear's axial height and overall volume; therefore, the VTD of the axial flux gears is maximized by choosing the appropriate intermediate PM thickness instead of simply using the largest permissible value. Similarly, Fig. 3(b) reveals that the PM GTD is maximized for each topology and outer radius combination by choosing the minimum magnet thickness considered in the study to minimize the effective air gap and use the magnet material as effectively as possible. The theoretically optimal magnet thicknesses for maximizing PM GTD would likely be impractically thin for manufacturing and handling.

It is important to note that because magnetic gears have large linear reluctances from the two air gaps and two sets of PMs, their design often favors a higher degree of saturation than typical electric machines, which have much smaller linear reluctances. For some of the highest VTD designs, flux densities reached peak levels of almost 2.5 T in the Rotor 1 back iron, approximately 1.75 T in the modulators, and nearly 2.5 T in the Rotor 3 back iron. For some of the highest PM GTD designs, flux densities reached peak levels of almost 1.75 T in the Rotor 1 back iron, approximately 1.15 T in the modulators, and nearly 2.25 T in the Rotor 3 back iron. Despite these high flux densities, magnetic gears can achieve high efficiencies, especially under high torque, low speed operating conditions [24]. While these high iron flux densities do cause some core losses, the eddy current losses in the PMs often account for the majority of the total losses in a magnetic gear, especially as the operating speed increases [5], [24], and laminated PMs can be used to improve the efficiency if necessary.

Fig. 4 demonstrates that the Rotor 1 pole pair sweep ranges summarized in Table IV contain the optimum values for both VTD and PM GTD at each of the design scenarios indicated in the legend in Fig. 2, except for the 50 mm outer radius maximum VTD design set. The VTD for this design set would be maximized by using a Rotor 1 pole pair count of less than 3; however, as indicated in Table IV, Rotor 1 pole pair counts below 3 were not considered in the study because they generally lead to high torque ripple unless additional measures, such as magnet skewing, are employed [4]. In general, the results in Fig. 4 suggest the fairly obvious conclusion that the larger outer radius designs favor higher pole pair counts than the lower outer radius designs.

A comparison of the graphs in Fig. 4(a) and Fig. 4(b) also indicates that the maximum PM GTD designs use higher Rotor 1 pole pair counts than the maximum VTD designs. This is because the thicker magnets used in the maximum VTD designs increase the effective air gaps, which results in increased leakage flux between adjacent poles. This must be counteracted by using lower pole pair counts to achieve larger pole arcs [25]. Fig. 5 illustrates this principle by depicting the impact of the Rotor 1 magnet thickness on the optimal Rotor 1 pole pair count that maximizes the average low speed air gap shear stress (indicated by the dashed line) in axial flux gears and 50 mm stack length radial flux gears with 200 mm outer radii and $G_{Int} = 4$.

The results in Fig. 6 reveal that increasing the gear ratio yields lower maximum VTDs and PM GTDs for both the axial and radial flux topologies. This is primarily because the larger gear ratio increases the disparity between the pole pair counts on the different rotors, which makes it more difficult to simultaneously optimize the pole pair counts on each rotor. As illustrated by the curves in Figs. 6(b) and 6(d), higher gear ratio designs favor lower Rotor 1 pole pair counts in order to decrease the Rotor 3 pole pair and modulator counts and decrease leakage flux in those regions; however, that leads to decreased coenergy derivatives with respect to rotor positions. Consequently, both VTD and PM GTD tend to decrease as the gear ratio increases (within the evaluated range), and the resulting optimums (maximum torque densities) depicted in Fig. 6 represent compromises between these competing influences at each design point.

B. 3-D Scaling Design Parameters

Figs. 8-10 depict the variation of the design quality metrics with the outer radius, stack length, and radii ratio for each of the various G_{Int} value and topology combinations denoted in the legend in Fig. 7. Fig. 8 shows how the maximum torque density values scale with the gear's outer radius, which is one of the most noteworthy differences between the axial flux and radial flux topologies. As predicted by the analysis summarized in Table I, the VTD of the axial flux gears grows almost linearly with the outer radius. On the other hand, while Table I suggests that the VTD of radial flux gears is ideally invariant with the outer radius, the results in Fig. 8(a) demonstrate that it actually increases at a diminishingly sublinear rate with the outer radius (due to several considerations not accounted for in Table I). One basic major factor causing this growth is that the ratio of the air gap radius to the outer radius increases as the outer radius increases. Another important consideration for both radial flux and axial flux gears is that higher outer radius designs favor larger pole counts, as previously indicated in Fig. 4, which means that there is finer resolution (on a percent change basis) for better optimization between consecutive discrete pole pair count values. Furthermore, as previously noted, the lowest pole pair count considered, 3, is sub-optimal for maximizing VTD at an outer radius of 50 mm. Regardless, axial flux magnetic gears are able to achieve significantly higher VTDs than radial flux gears at relatively larger outer radii but achieve lower VTDs than radial flux gears at lower outer radii. However, the PM GTDs tend to scale approximately linearly with outer radius for each topology. Since the PM mass is approximately proportional to the air gap area, this is consistent with

behavior predicted by the analysis in Table I. Additionally, Fig. 8 reinforces the observation that the designs with larger gear ratios tend to perform worse (within the evaluated range of gear ratios).

Fig. 8 also shows that the 3D FEA predicts a lower torque for the radial flux designs than the 2D FEA, which is due to the magnetic gears' end-effects [29]. Fig. 9 compares the difference between the 2D FEA results and the 3D FEA

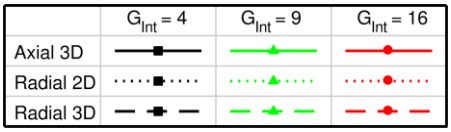

Fig. 7. Legend for Figs. 8-10.

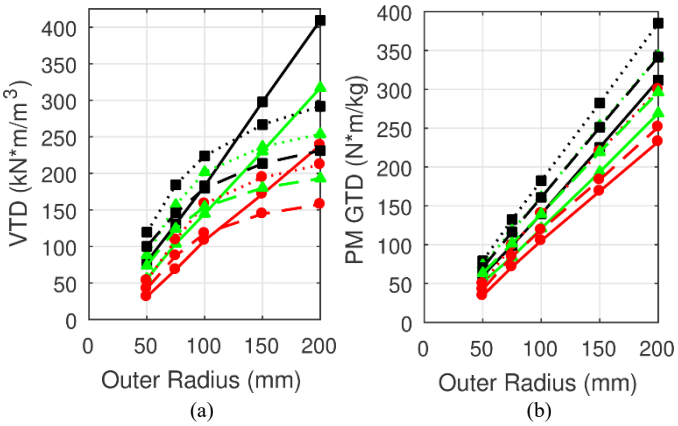

Fig. 8. Variation of maximum (a) VTD and (b) PM GTD with outer radius for both axial flux gears and 50 mm stack length radial flux gears at different G_{Int} values.

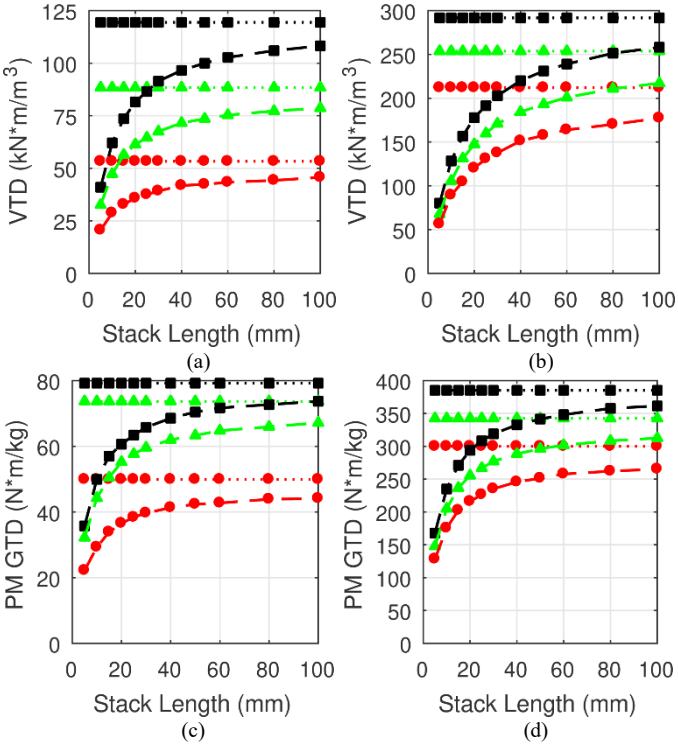

Fig. 9. Variation of (a) maximum VTD at a 50 mm outer radius, (b) maximum VTD at a 200 mm outer radius, (c) maximum PM GTD at a 50 mm outer radius, and (d) maximum PM GTD at a 200 mm outer radius with stack length for radial flux gears at different G_{Int} values (based on 2D and 3D FEA).

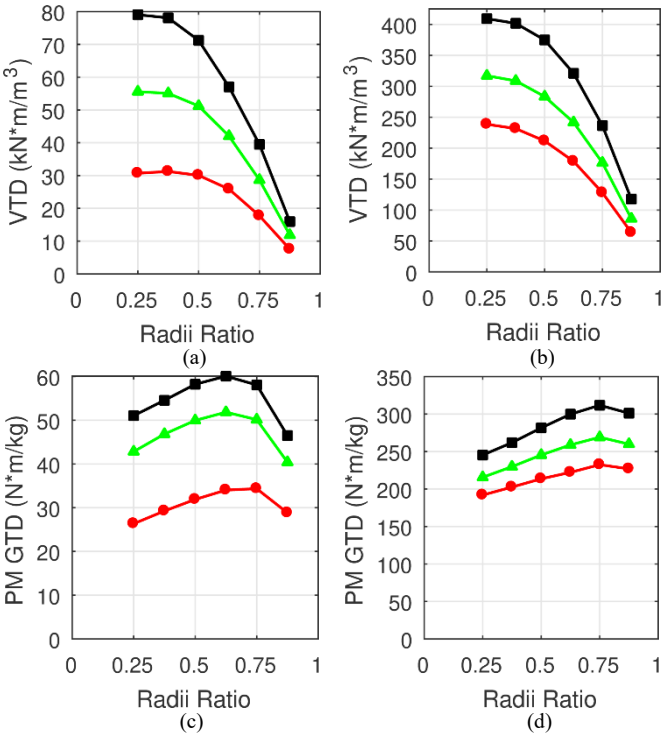

Fig. 10. Variation of (a) maximum VTD at a 50 mm outer radius, (b) maximum VTD at a 200 mm outer radius, (c) maximum PM GTD at a 50 mm outer radius, and (d) maximum PM GTD at a 200 mm outer radius with radii ratio for axial flux gears at different G_{Int} values.

results at different stack lengths, outer radii, and gear ratios, which leads to a few conclusions. First, the relative impact of the end-effects decreases as the stack length increases, with the 2D FEA VTD and PM GTD representing the ideal limits for the 3D FEA results as the stack length is increased indefinitely. This means that, for a given outer radius, designs with higher torque ratings (and, thus, longer stack lengths) will tend to have higher VTDs and PM GTDs than designs with lower torque ratings. Second, the end-effects tend to have a more significant impact on the maximum VTD designs than on the maximum PM GTD designs. This is likely due to the aforementioned facts that the maximum VTD designs have much thicker magnets, which increases both the effective air gap and the impact of the escaping flux, and lower pole pair counts, which leads to longer flux paths and more axially escaping leakage flux [29]. Finally, the stack length has a much stronger influence on the impact of end-effects than the outer radius (assuming that the other parameters, such as pole counts are optimized independently for each radius).

The impact of the radii ratio on an axial flux gear's performance, which is depicted in Fig. 10, is more complex than the impact of the stack length on a radial flux gear's performance. Fig. 10 illustrates that relatively low radii ratios produce higher VTDs, whereas relatively high radii ratios produce higher PM GTDs, especially at larger outer radii. Reducing the radii ratio increases the portion of the total volume of the gear that is being used to produce torque. However, Fig. 10 shows that the VTD returns diminish as the radii ratio is reduced. There are a few reasons for this. First, as the radii ratio is reduced, the increase in the active air gap area diminishes, because the new active material is added at a

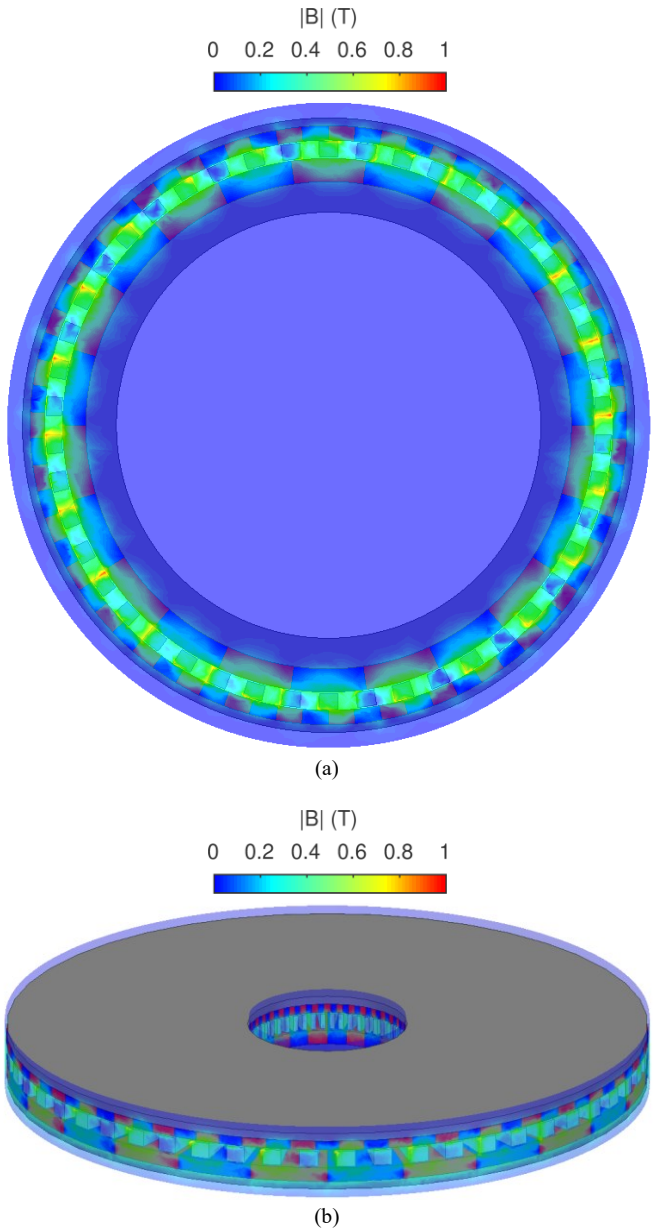

Fig. 11. Magnetic flux densities (a) 1 mm axially beyond the stack of the radial flux design with the highest VTD and (b) 1 mm radially inside the inner radius and 1 mm radially outside the outer radius of the axial flux design with the highest VTD.

diminishingly smaller radius (assuming a fixed outer radius). Additionally, because the added material is placed at a lower radius, it has a smaller lever arm. Finally, a single P_1 value is only optimal for a small range of radii. Thus, a single P_1 value cannot be simultaneously optimal at the gear's outer and inner radii. As the radii ratio decreases, the degree of this sub-optimality increases. For these reasons, the maximum PM GTD designs tend to have higher radii ratios to optimize the use of the PM material. Nonetheless, the PM GTD is not simply maximized by raising the radii ratio to unity because the impact of end-effects (radial leakage flux) increases as the radii ratio increases and the active material becomes radially thinner. However, as illustrated by Figs. 10(c) and 10(d), the radii ratio that maximizes PM GTD increases slightly as the outer radius increases.

While the radial flux gear experiences end-effects near its axial top and bottom, as illustrated by the flux plot in Fig. 11(a), the axial flux gear experiences end-effects near its radial inner and radial outer surfaces, as illustrated by the flux plot in Fig. 11(b). In both topologies, the flux densities outside the gear tend to be highest in areas axially or radially beyond the modulators at angular positions where the PMs on Rotor 1 and Rotor 3 are magnetized in the opposite directions.

Changing the radial flux gear stack length scales the 2-D r-θ cross-section along the axial dimension. This has minimal impact on the optimal parameter values, except for a minor change in the optimal magnet thicknesses when optimizing for some metrics [25]. However, changing the axial flux gear radii ratio scales the 2-D θ-z cross-section along the radial dimension, which has a more significant impact on the optimal parameter values because it fundamentally impacts the flux path lengths. Fig. 12 illustrates the impact of the radii ratio on the optimal Rotor 1 pole pair counts (indicated by the dashed line) for axial flux designs with an outer radius of 200 mm and $G_{Int} = 4$. As indicated by Fig. 12, the optimal pole counts tend to decrease as the radii ratio decreases (for a fixed outer radius) because the effective average radius of the air gap decreases, which makes lower pole counts more optimal (as previously shown in Fig. 4). Similar trends are present for other outer radius and gear ratio combinations, but they are less pronounced because lower outer radii or higher gear ratios tend to already favor lower Rotor 1 pole pair counts.

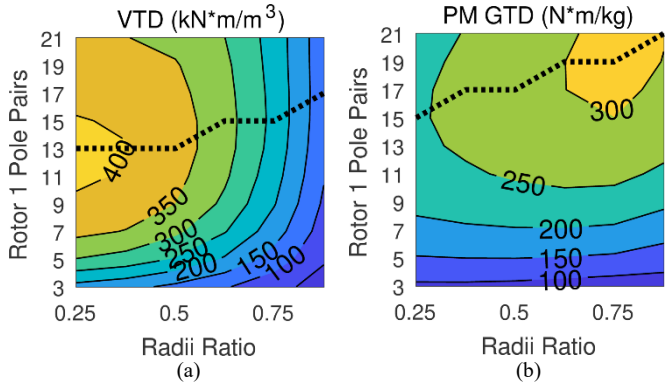

Fig. 12. Variation of maximum (a) VTD and (b) PM GTD with radii ratio and Rotor 1 pole pair count for axial flux gears (with a 200 mm outer radius and $G_{Int} = 4$). The dashed line indicates the optimal Rotor 1 pole pair count for each radii ratio.

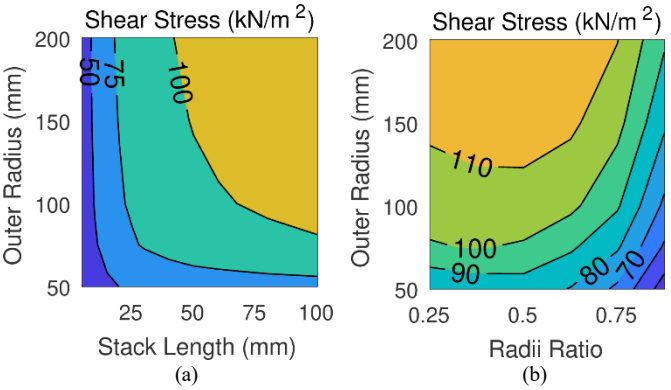

Fig. 13. Variation of maximum average low speed air gap shear stress for (a) radial flux gears and (b) axial flux gears (both with $G_{Int} = 4$).

Fig. 13 illustrates the maximum average shear stress in the low speed air gaps for both radial and axial flux designs with G_{Int} = 4. Fig. 13(a) shows that, for radial flux designs, shear stress increases with both stack length and outer radius. As the stack length increases, the impact of end-effects becomes less significant, resulting in higher average shear stress. The increase in shear stress with outer radius contributes to the sublinear increase in VTD with outer radius previously shown for radial flux gears in Fig. 8(a). For axial flux gears, Fig. 13(b) shows that shear stress increases with outer radius but is maximized at an intermediate radii ratio slightly below 0.5. If the radii ratio is too low, the best P_1 value will be suboptimal for a significant portion of the air gap area, but, if the radii ratio is too high, the impact of end effects on the stall torque will be very significant. For both topologies, the shear stress tends to increase with the outer radius because, as previously noted, the designs can use more optimal pole counts at higher outer radii. Fig. 13 also shows that both topologies are able to achieve approximately the same shear stresses.

C. Torques and Forces

Fig. 14 shows the Rotor 2 stall torques for the design points used to create Fig. 13. For both topologies, shear stress tends to increase with outer radius, but the Rotor 2 stall torque tends to increase even faster with outer radius. Thus, the achievable shear stress tends to increase as the torque rating increases, but with diminishing returns. For the radial flux gears, a similar trend is present as stack length increases. Thus, based on Figs. 8-14, applications requiring larger torques will be able to achieve higher shear stresses, VTDs, and PM GTDs than applications where the rated torque is much smaller.

Another major difference between radial flux and axial flux gears is the magnetic forces upon the rotors. While symmetry can ideally be used to cancel out the net radial magnetic forces on a radial flux gear rotor, each rotor in an axial flux gear will still experience unbalanced net axial magnetic forces. Fig. 15 illustrates the corresponding axial magnetic forces on Rotor 1 and Rotor 3 for each of the axial flux gear design points used to create Fig. 13(b). The axial magnetic forces shown in Fig. 15 are those at the stall torque points (orientations). While the stall torque points are not necessarily the maximum axial force points, they do give an indication of the axial forces experienced by the rotors in the different designs [17]. A comparison of Figs. 14(b) and 15 indicates that the designs with higher torques generally experience larger axial forces. However, the axial forces grow faster than the stall torque as the radii ratio decreases because, unlike the stall torque, the axial force created by a differential area of the air gap is independent of the lever arm of that differential area. Thus, the same stall torque can often be achieved with smaller axial forces by increasing both the outer radius and the radii ratio. While not shown in Fig. 15, the net axial force on Rotor 2 in a given design is simply the algebraic difference between the axial forces on Rotor 1 and Rotor 3 (in accordance with Newton's 3rd law). This means that the net axial force on Rotor 2 is generally much smaller than the net axial forces on Rotor 1 and Rotor 3.

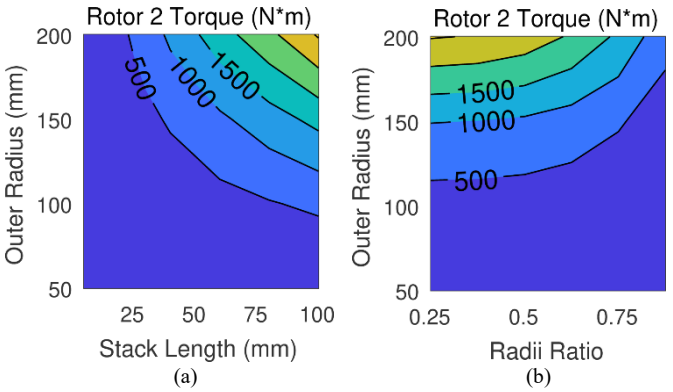

(a) (b)

Fig. 14. Rotor 2 stall torques corresponding to (a) the radial flux gear design points in Fig. 13(a) and (b) the axial flux gear design points in Fig. 13(b).

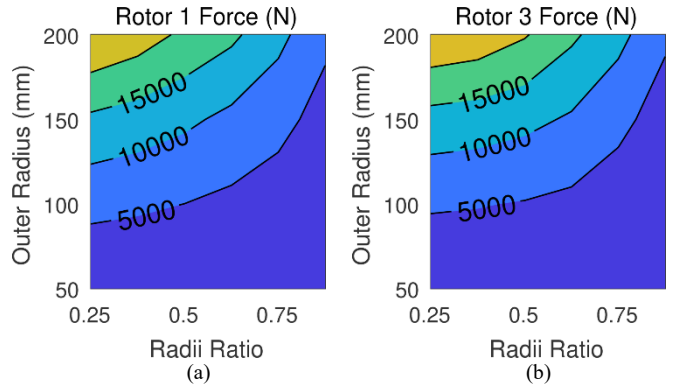

(a) (b)

Fig. 15. (a) Rotor 1 and (b) Rotor 3 axial magnetic forces corresponding to the stall torque alignments of the axial flux gear design points in Fig. 13(b).

IV. Conclusion

Radial flux and axial flux coaxial magnetic gears both provide gearing action without mechanical contact between rotors. Additionally, there are some significant similarities between their performances. Both topologies achieve higher VTDs and PM GTDs at higher torques and lower gear ratios (within the range of gear ratios evaluated). Also, the two topologies can achieve similar air gap shear stresses. However, there are some key performance differences.

First, while the achievable VTDs of both topologies tend to increase with outer radius, the achievable VTDs of axial flux gears grow faster than those of radial flux gears. Thus, the axial flux gear favors large outer radii with small axial lengths. However, the PM GTDs of the two topologies tend to increase at similar rates as the outer radius increases.

Furthermore, the impact of end-effects on the two topologies is different. For radial flux gears, the axial end-effects become less significant as the stack length increases, which raises both VTD and PM GTD, as well as torque. For axial flux gears, shear stress is maximized with an intermediate radii ratio, but VTD is maximized with a lower radii ratio. On the other hand, PM GTD is maximized at a higher radii ratio.

Finally, whereas the net radial magnetic forces on each rotor of a radial flux gear can ideally be eliminated, the net axial forces on the rotors of an axial flux gear cannot be eliminated. This presents a significant challenge for the construction of axial flux gears.

While the conclusions presented above will generally hold true, it is important to recognize that the exact numbers and the extent of the trends presented in this study depend on the assumptions made in setting up the simulations, as is the case for all design studies. First, all of the results presented in this paper are based on the assumption of equal 1 mm air gaps for both the axial flux and radial flux gears. In practice, the unbalanced axial forces on the rotors in axial flux gears may necessitate the use of larger air gaps in this topology, which would shift the results in favor of radial flux gears. On the other hand, radial flux gears may require a larger effective inner air gap to accommodate a retention sleeve for the Rotor 1 PMs, especially if the gear is designed for high Rotor 1 speeds. However, to retain the Rotor 1 PMs in axial flux gears, a ring or lip can be placed radially beyond these PMs, which does not contribute to the effective air gap. Furthermore, this study maintained a constant air gap size (1 mm) regardless of other design settings. In practice, the air gap will likely need to increase as the outer radius increases, which would reduce (but not eliminate) the VTD and PM GTD gains achieved by going to a larger outer radius. The exact scaling of this air gap increase will depend on design specific mechanical and manufacturing considerations. Additionally, the simulation models employed in this study used a soft magnetic composite for the modulators in both topologies, and switching to traditional laminated steel modulators could slightly raise the torque ratings of the best designs due to its higher saturation flux density. However, while laminated steel modulators are perfectly feasible for radial flux gears, they are less practical for axial flux gears. Thus, if axial flux gears are constructed using soft magnetic composite modulators and radial flux gears are constructed using laminated steel modulators, this would also shift the findings a little further in favor of radial flux gears. Even if these factors are not considered, based on the results of this study, radial flux gears will likely be superior to axial flux gears in most applications due to their simpler construction and higher performance at most physical form factors. However, axial flux gears have a significant potential advantage in applications where a large outer radius and a small axial length are permissible or where mechanical power needs to be transmitted across a flat barrier.

V. Acknowledgment

The authors would like to thank ANSYS for their support of the EMPE lab through the provision of FEA software.

VI. References

[1] K. Atallah and D. Howe, “A novel high-performance magnetic gear,” *IEEE Trans. Magn.*, vol. 37, no. 4, pp. 2844–2846, Jul. 2001.

[2] P. O. Rasmussen, T. O. Anderson, F. T. Jorgensen, and O. Nielsen, “Development of a High Performance Magnetic Gear,” *IEEE Trans. Ind. Appl.*, vol. 41, no. 3, pp. 764-770, May/June 2005.

[3] P. M. Tlali, R.-J. Wang, and S. Gerber, “Magnetic gear technologies: A review,” *Proc. Int. Conf. Elect. Mach.*, 2014, pp. 544–550.

[4] N. W. Frank and H. A. Toliyat, “Gearing ratios of a magnetic gear for wind turbines,” *Proc. IEEE Int. Elect. Mach. and Drives Conf.*, 2009, pp. 1224–1230.

[5] M. Johnson, M. C. Gardner, H. A. Toliyat, S. Englebretson, W. Ouyang, and C. Tschida, "Design, Construction, and Analysis of a Large Scale Inner Stator Radial Flux Magnetically Geared Generator for Wave Energy Conversion," *IEEE Trans. Ind. Appl.*, vol. 54, no. 4, pp. 3305-3314, July/Aug 2018.

[6] K. K. Uppalapati, J. Z. Bird, D. Jia, J. Garner, and A. Zhou, “Performance of a magnetic gear using ferrite magnets for low speed ocean power generation,” in *Proc. IEEE Energy Convers. Congr. and Expo.*, 2012, pp. 3348–3355.

[7] T. V. Frandsen, L. Mathe, N. I. Berg, R. K. Holm, T. N. Matzen, P. O. Rasmussen, and K. K. Jensen, “Motor integrated permanent magnet gear in a battery electrical vehicle,” *IEEE Trans. Ind. Appl.*, vol. 51, no. 2, pp. 1516–1525, Mar./Apr. 2015.

[8] L. MacNeil, B. Claus, and R. Bachmayer, “Design and evaluation of a magnetically-geared underwater propulsion system for autonomous underwater and surface craft,” in *Proc. Int. Conf. IEEE Oceans*, 2014, pp. 1-8.

[9] S. Mezani, K. Atallah, and D. Howe, “A high performance axial-field magnetic gear,” *J. Appl. Phys.*, vol. 99, 08R303, 2006.

[10] T. Lubin, S. Mezani, and A. Rezzoug, “Development of a 2-D Analytical Model for the Electromagnetic Computation of Axial-Field Magnetic Gears,” *IEEE Trans. Magn.*, vol. 49, no. 11, pp. 5507-5521, Nov. 2013.

[11] V. M. Acharya, J. Z. Bird, and M. Calvin, “A Flux Focusing Axial Magnetic Gear,” *IEEE Trans. Magn.*, vol. 49, no. 7, pp. 4092-4095, July 2013.

[12] M. Johnson, M. C. Gardner, and H. Toliyat, “Analysis of Axial Field Magnetic Gears with Halbach Arrays,” in *Proc. IEEE Int. Elect. Mach. and Drives Conf.*, 2015, pp 108-114.

[13] M. Johnson, A. Shapoury, P. Boghrat, M. Post, and H. A. Toliyat, “Analysis and development of an axial flux magnetic gear,” in *Proc. IEEE Energy Convers. Congr. and Expo*, 2014, pp. 5893-5900.

[14] K. Atallah, J. Rens, S. Mezani, and D. Howe, “A novel ‘pseudo’ direct-drive brushless permanent magnet machine,” *IEEE Trans. Magn.*, vol. 44, no. 11, pp. 4349-4352, Nov. 2008.

[15] L. Jian, K. T. Chau, and J. Z. Jiang, “A magnetic-geared outer-rotor permanent-magnet brushless machine for wind power generation,” *IEEE Trans. Ind. Appl*., vol. 35, no. 3, pp. 954–92, May/Jun. 2009.

[16] S. Gerber and R.-J. Wang, “Design and evaluation of a disc-type magnetically geared PM wind generator,” in *Proc. 4th Int. Conf. Power Eng. Energy Elect. Drives*, Istanbul, Turkey, May 2013, pp. 1259-1264.

[17] M. Johnson, M. C. Gardner and H. A. Toliyat, “Design and Analysis of an Axial Flux Magnetically Geared Generator,” *IEEE Trans. Ind. Appl.*, vol. 53, no. 1, pp. 97-105, Jan./Feb. 2017.

[18] K. Atallah, S. D. Calverley, and D. Howe, “Design, analysis and realisation of a high-performance magnetic gear,” *IEE Proc. - Electr. Power Appl.*, vol. 151, no. 2, pp. 135–143, Mar. 2004.

[19] S. Gerber and R. J. Wang, “Design and Evaluation of a Magnetically Geared PM Machine,” *IEEE Trans. Magn.*, vol. 51, no. 8, pp. 1-10, Aug. 2015.

[20] T. V. Frandsen, P. O. Rasmussen and K. K. Jensen, “Improved motor intergrated permanent magnet gear for traction applications” in *Proc. IEEE Energy Convers. Congr. and Expo.*, 2012, pp. 3332-3339.

[21] G. Jungmayr, J. Loeffler, B. Winter, F. Jeske, and W. Amrhein, "Magnetic Gear: Radial Force, Cogging Torque, Skewing, and Optimization," *IEEE Trans. Ind. Appl.*, vol. 52, no. 5, pp. 3822-3830, Sept./Oct. 2016.

[22] A. Rahideh, A. A. Vahaj, M. Mardaneh, and T. Lubin, "Two-dimensional analytical investigation of the parameters and the effects of magnetisation patterns on the performance of coaxial magnetic gears," *IET Elec. Syst. Transp.*, vol. 7, no. 3, pp. 230-245, 9 2017.

[23] Y. Chen, W. N. Fu, S. L. Ho, H. Liu, “A Quantitative Comparison Analysis of Radial-Flux, Transverse-Flux, and Axial-Flux Magnetic Gears,” *IEEE Trans. Magn.*, vol. 50, no. 11, pp. 1-4, Nov. 2014.

[24] M. Johnson, M. C. Gardner, and H. A. Toliyat, “Design Comparison of NdFeB and Ferrite Radial Flux Surface Permanent Magnet Coaxial Magnetic Gears,” *IEEE Trans. Ind. Appl.*, vol. 54, no. 2, pp. 1254 – 1263, Mar./Apr. 2018.

[25] M. C. Gardner, B. E. Jack, M. Johnson, and H. A. Toliyat, “Comparison of Coaxial Radial Flux Magnetic Gears Independently Optimized for

Volume, Cost, and Mass," *IEEE Trans. Ind. Appl.*, vol. 54, no. 3, pp. 2237-2245, May/June 2018.

[26] D. J. Evans and Z. Q. Zhu, "Influence of design parameters on magnetic gear's torque capability," in *Proc. IEEE Int. Elect. Mach. Drives Conf.*, 2011, pp. 1403-1408.

[27] D. J. Patterson, J. L. Colton, B. Mularcik, B. J. Kennedy, S. Camilleri, and R. Rohoza, "A comparison of radial and axial flux structures in electrical machines," *in Proc. IEEE Int. Elect. Mach. and Drives Conf.*, 2009, pp. 1029-1035.

[28] A. Penzkofer and K. Atallah, "Scaling of Pseudo Direct Drives for Wind Turbine Application," *IEEE Trans. Magn.*, vol. 52, no. 7, pp. 1-5, July 2016.

[29] S. Gerber and R-J. Wang, "Analysis of the end-effects in magnetic gears and magnetically geared machines," in *Proc. IEEE Int. Conf. Elect. Mach.*, 2014, pp. 396-402.

VII. BIOGRAPHIES

Matthew C. Gardner (S' 15) earned his B.S. in electrical engineering with a minor in Computer Science from Baylor University, Waco, Texas in 2014. He is currently pursuing a Ph.D. in electrical engineering while working in the Advanced Electric Machines and Power Electronics Laboratory at Texas A&M University. His research interests include optimal design and control of magnetic gears and magnetically geared machines.

Matthew Johnson (S' 13, M'17) earned his B.S. in electrical engineering with a minor in mathematics from Texas A&M University, College Station, Texas in 2011. In 2017, he received a Ph.D. in electrical engineering while working in the Advanced Electric Machines and Power Electronics Laboratory at Texas A&M University. His research interests include magnetic gears, magnetically geared machines, and motor drives.

Hamid A. Toliyat (S'87, M'91, SM'96, F'08) received the B.S, degree from Sharif University of Technology, Tehran, Iran in 1982, the M.S. degree from West Virginia University, Morgantown, WV in 1986, and the Ph.D. degree from University of Wisconsin-Madison, Madison, WI in 1991, all in electrical engineering. Following receipt of the Ph.D. degree, he joined the faculty of Ferdowsi University of Mashhad, Mashhad, Iran as an Assistant Professor of Electrical Engineering. In March 1994 he joined the Department of Electrical and Computer Engineering, Texas A&M University where he is currently the Raytheon endowed professor of electrical engineering. Dr. Toliyat has many papers and awards to his name, including the Nikola Tesla Field Award.